RESEARCH ARTICLE

Figures and figure supplements

Systematic analysis of the molecular and biophysical properties of key DNA damage response factors

Joshua R Heyza *et al*.

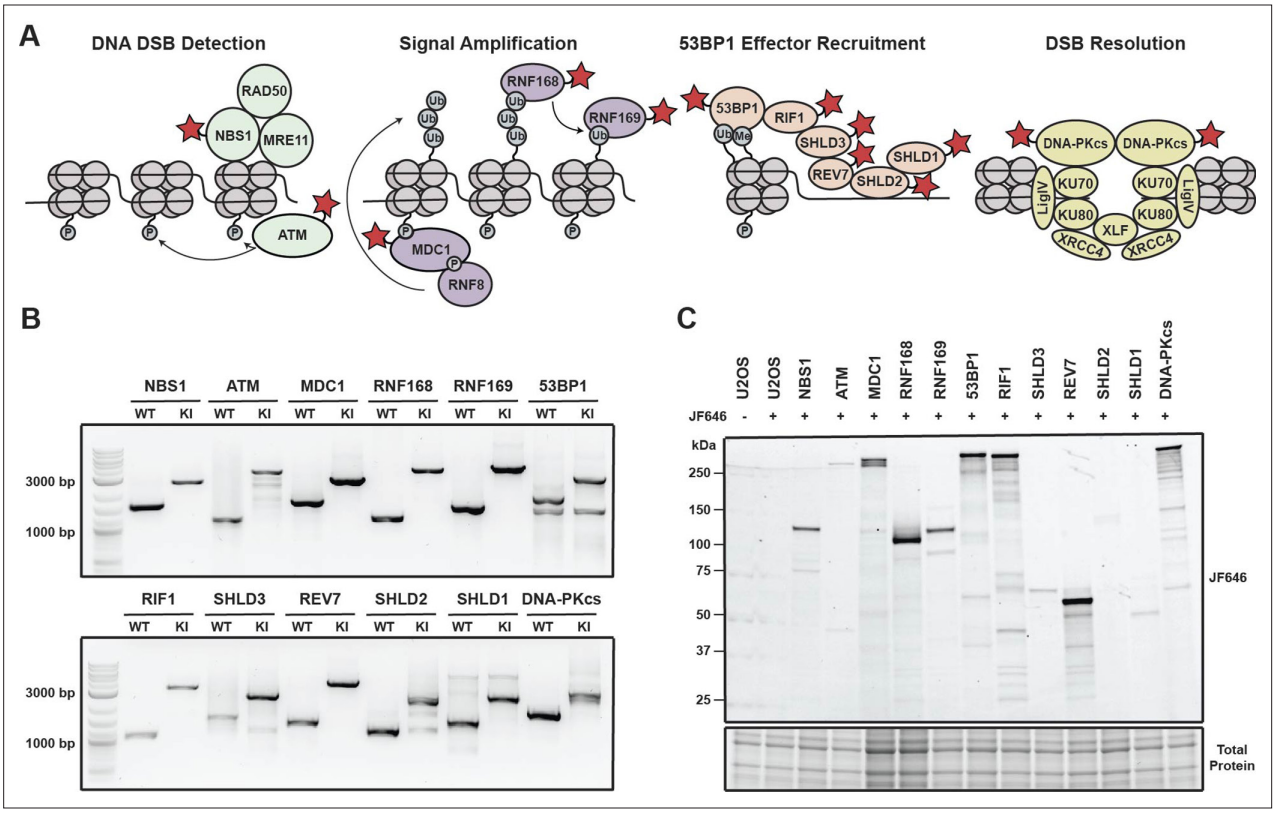

Figure 1. Generation of a panel HaloTagged DNA damage response proteins with CRISPR-Cas9 and homology-directed repair. (**A**) Model of the DDR factors HaloTagged by genome editing and their roles in DSB repair. Red star indicates HaloTagged protein. (**B**) Agarose gels depicting PCR products amplified from genomic DNA showing insertion of the 3xFLAG-HaloTag into the genomic loci of each tagged DDR factor using primers oriented outside of both left and right homology arms. (WT = wildtype; KI = knock in) (**C**) SDS-PAGE gel showing fluorescently labeled HaloTagged proteins in each cell line after labeling with JF646 HaloTag ligand.

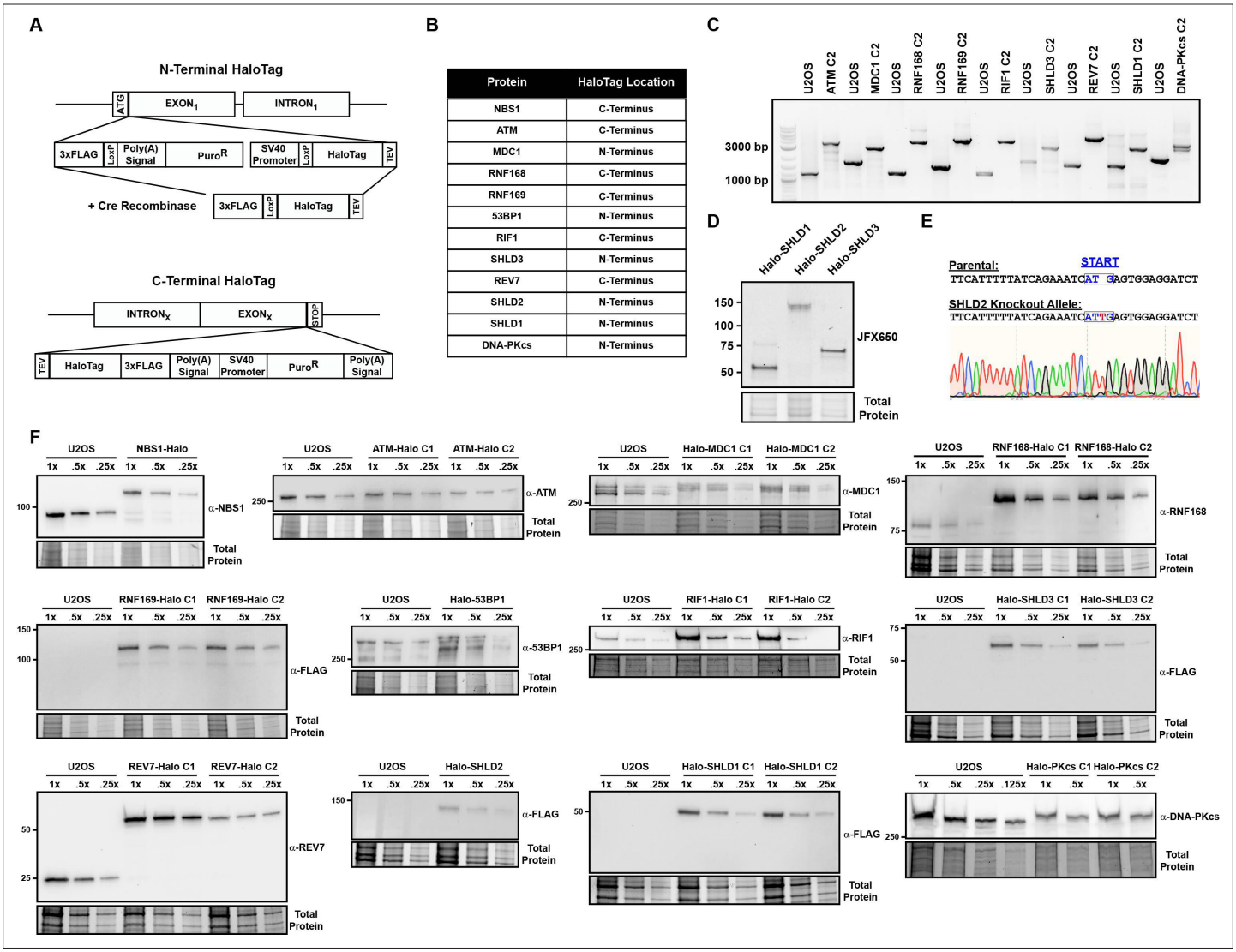

Figure 1—figure supplement 1. HaloTag knock-in design and knock-in validation. (**A**) Graphical representation of the N-terminal and C-Terminal 3xFLAG-HaloTag used for genome editing. (**B**) Table indicating the terminus where the HaloTag was introduced for each protein (**C**) Agarose gel showing genomic PCR products and HaloTag insertion for second knock-in clones using primers oriented outside of the left and right homology arms. (**D**) SDS-PAGE gel of fluorescently tagged SHLD1, SHLD2, and SHLD3 with higher exposure than the gel presented in ***Figure 1C***. (**E**) Sanger sequencing of the knockout allele of SHLD2 where the Start codon is highlighted in blue and the red indicated the single nucleotide insertion. (**F**) Western blots for HaloTagged DDR proteins showing relative expression of each tagged protein compared to parental U2OS cells for proteins where a commercially available antibody was both available and capable of detecting endogenous expression levels. For proteins where protein-specific antibodies were not available, proteins were probed with anti-FLAG antibody.

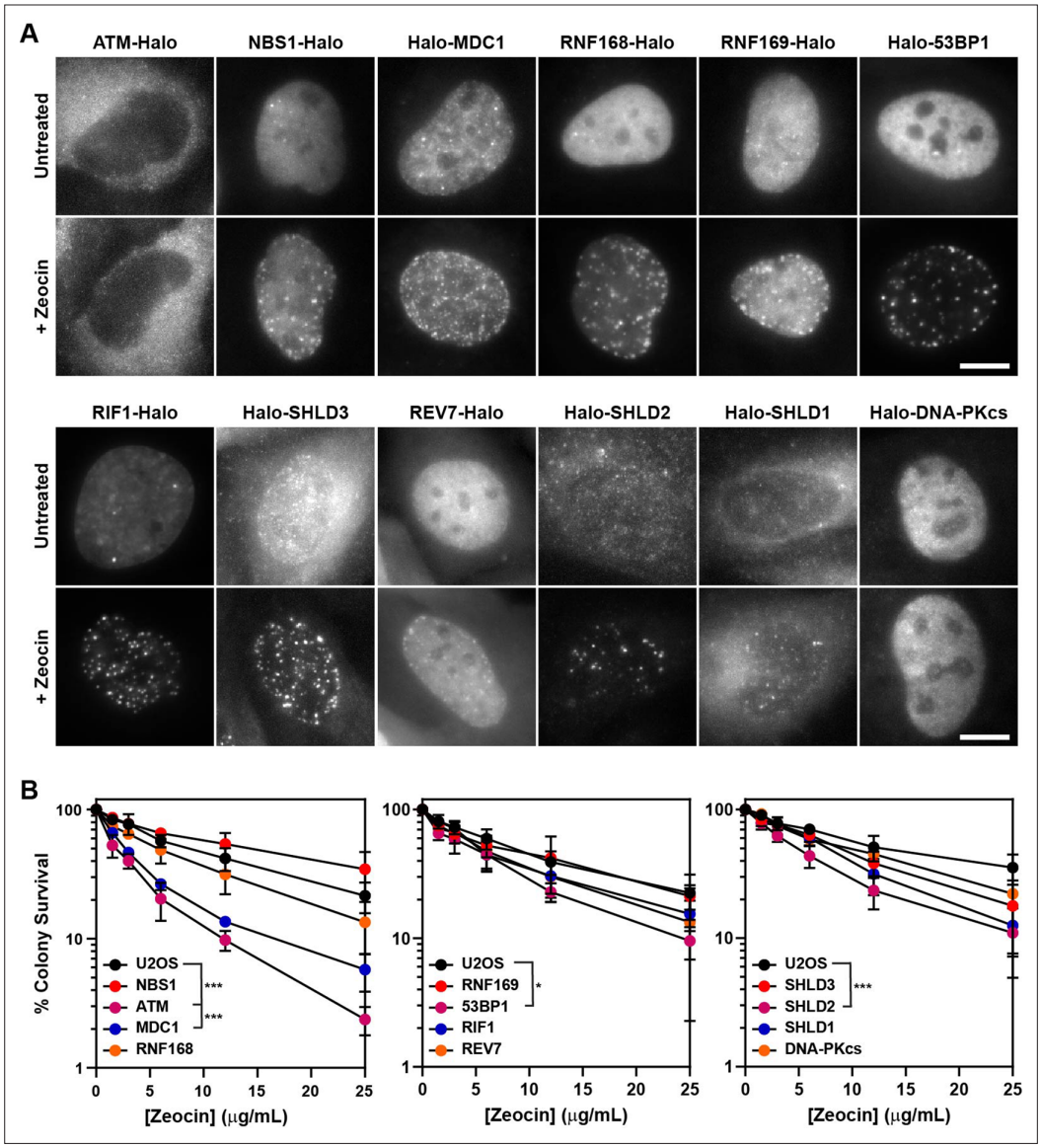

Figure 2. HaloTagged DDR proteins retain proper subcellular localization, foci-forming ability, and are competent for DNA repair. (**A**) Representative images of JF646-labeled HaloTagged proteins in the absence or presence of Zeocin in living cells. Data presented show protein cellular localization and foci-forming ability. Scale bar = 10 μm. Images are scaled differently between untreated and treated samples to demonstrate both localization and foci-forming ability. (**B**) Clonogenic survival assays representing the Zeocin-sensitivity of each HaloTagged DDR cell line relative to untagged parental U2OS cells. Data presented are the results of at least three independent experiments each plated in triplicate ± S.D. Data were compared by one-way ANOVA with Dunnett's posthoc test. * $p<0.05$; *** $p<0.001$.

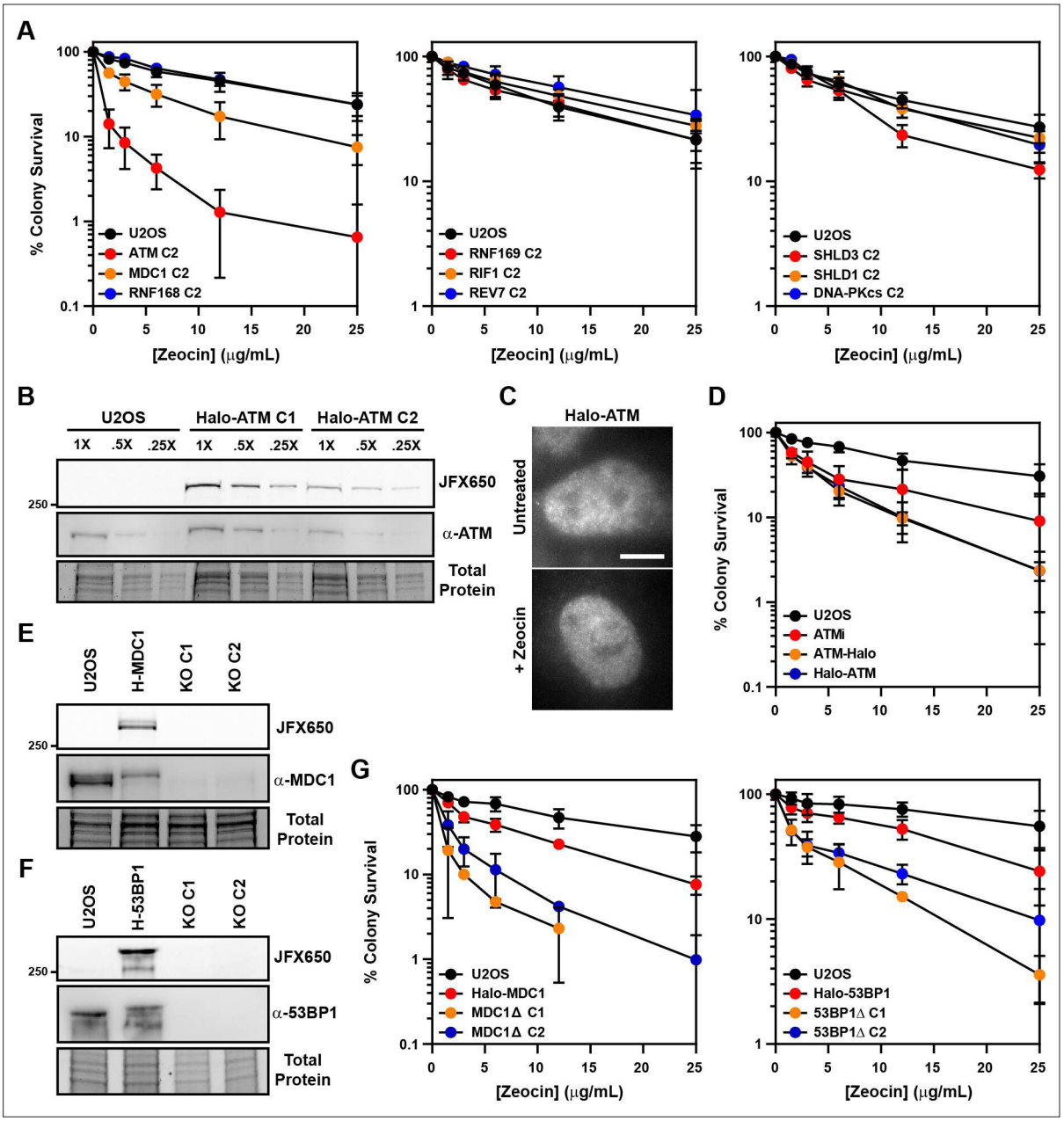

Figure 2—figure supplement 1. Functional validation of HaloTagged DDR proteins. (**A**) Clonogenic survival assay showing sensitivity of second HaloTag clones to Zeocin relative to parental U2OS cells. (**C**) SDS-PAGE and Western blot showing expression of N-terminally HaloTagged ATM. (**C**) Representative image of live cells expressing Halo-ATM in the presence or absence of Zeocin. Scale bar = 10 μm.(**D**) Clonogenic survival assays in the presence of absence of 10 μm ATMi (KU-55933) indicating that HaloTagging at either terminus abolishes ATM-mediated resistance to Zeocin. (**E & F**) SDS-PAGE and Western blot showing absence of Halo-MDC1 (H-MDC1) or Halo-53BP1 (H-53BP1) expression in MDC1 and 53BP1 knockout cells. (**G**) Clonogenic survival assays of MDC1 and 53BP1 knockout clones showing sensitivity to Zeocin relative to Halo-MDC1 or Halo-53BP1 and U2OS cells. Clonogenic survival assays are presented as the average ± S.D. of at least three independent experiments performed in triplicate. Data compared by one-way ANOVA with Dunnett's posthoc test. * $p<0.05$; ** $p<0.01$.

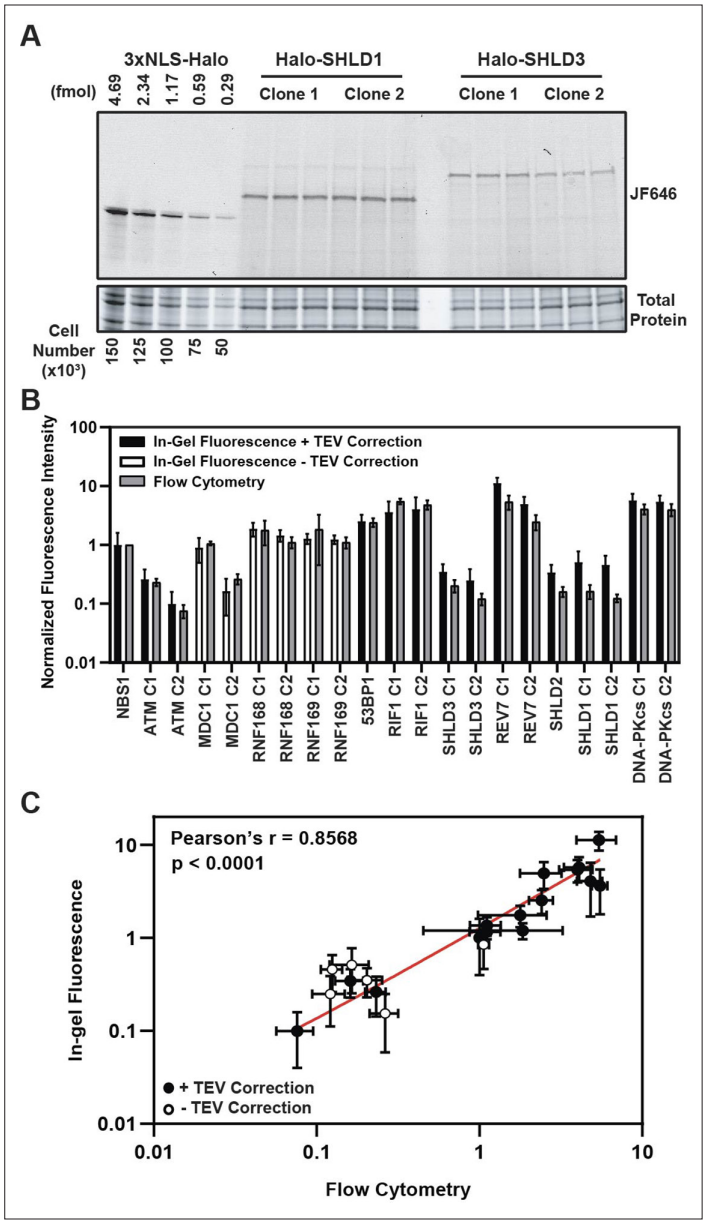

Figure 3. HaloTag enables quantification of absolute cellular protein abundances. (**A**) Example image of in-gel fluorescence of JF646-labeled HaloTagged proteins. (**B**) Comparison of JF646 fluorescence intensity values (normalized to NBS1-Halo) between in-gel fluorescence after applying the TEV correction factor and flow cytometry. White columns indicate unadjusted samples because of the inability to accurately determine a TEV correction factor due to protein degradation. Data are presented as the mean of ≥ three independent experiments ± S.D. (**C**) Plot representing the correlation of normalized JF646 fluorescence intensities ± S.D. for each protein between TEV-corrected in-gel fluorescence and flow-cytometry. Data were analyzed by Pearson's correlation coefficient. White points indicate those proteins for which a TEV-correction factor could not be accurately determined. Red line represents an interpolated standard curve.

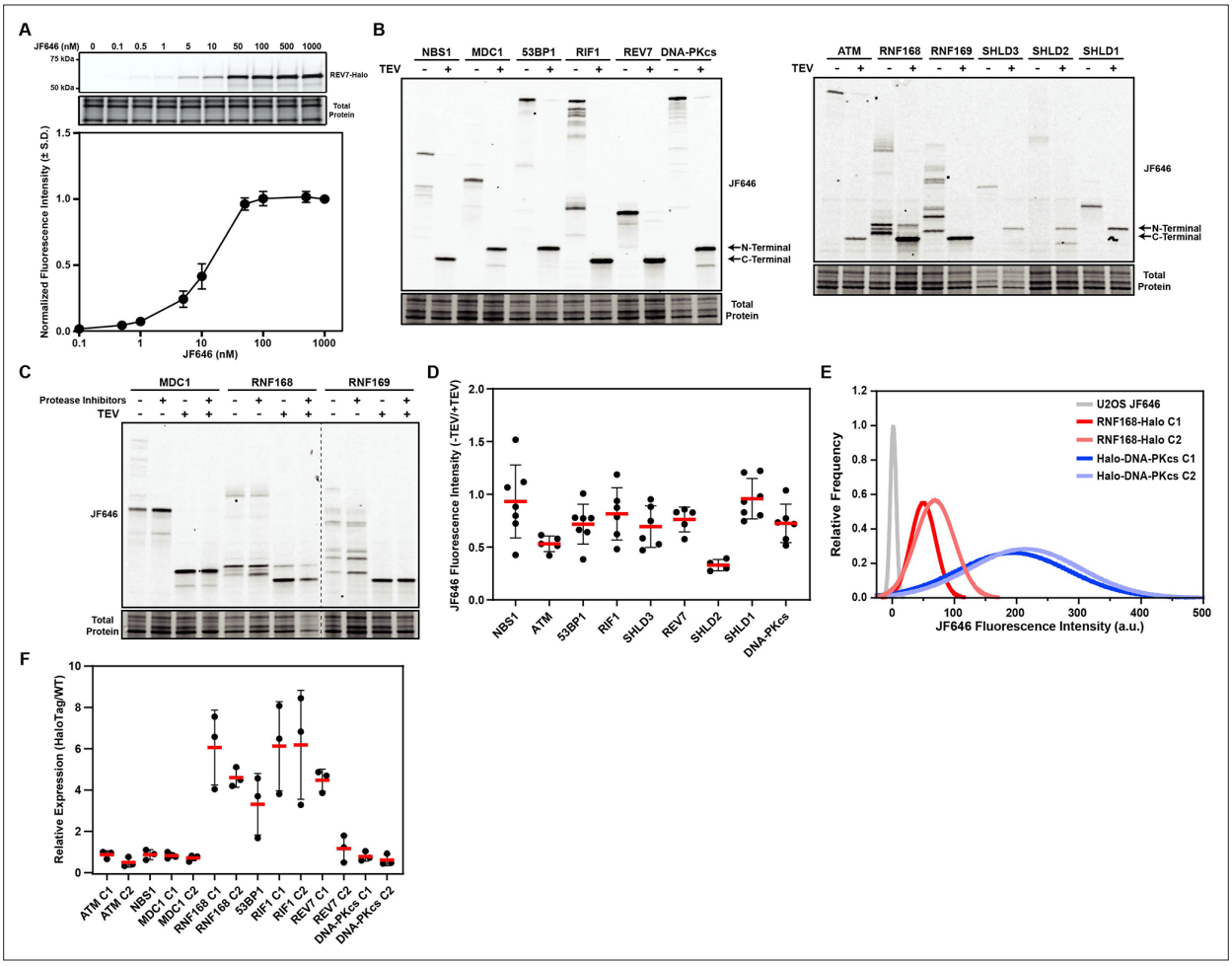

Figure 3—figure supplement 1. Quantification of absolute protein abundance using HaloTagged DDR proteins. (**A**) HaloTag labeling of REV7-Halo in cells titrated with increasing concentrations of JF646 with an associated saturation curve. Saturation curve data is plotted as the mean ± S.D. from three independent experiments. (**B**) Representative in-gel fluorescence images for TEV-digestion experiments used to generate an adjustment factor for protein abundance based upon JF646 signal intensity. N-terminal refers to the N-terminal 3XFLAG-HaloTag and C-Terminal refers to the C-terminal 3XFLAG-HaloTag. (**C**) In-gel fluorescence showing protein degradation products of MDC1, RNF168, and RNF169 in the presence or absence of protease inhibitor cocktail after lysing in CHAPS lysis buffer. (**D**) Quantification of TEV digestion experiments generating a TEV adjustment factor for absolute protein abundance. Each data point represents and independent experiment. Red bar indicates the mean and error bars represent S.D. (**E**) Representative plots of JF646 fluorescence intensity in parental U2OS cells, two RNF168-Halo clones, and two Halo-DNA-PKcs clones detected by flow cytometry. (**F**) Quantification of expression of HaloTagged protein relative to untagged protein in U2OS cells to generate a correction factor which was used to calculate the number of molecules per cell for each protein in wild-type U2OS cells. Data are quantified from three independent experiments. Red bar indicates the mean and error bars represent S.D.

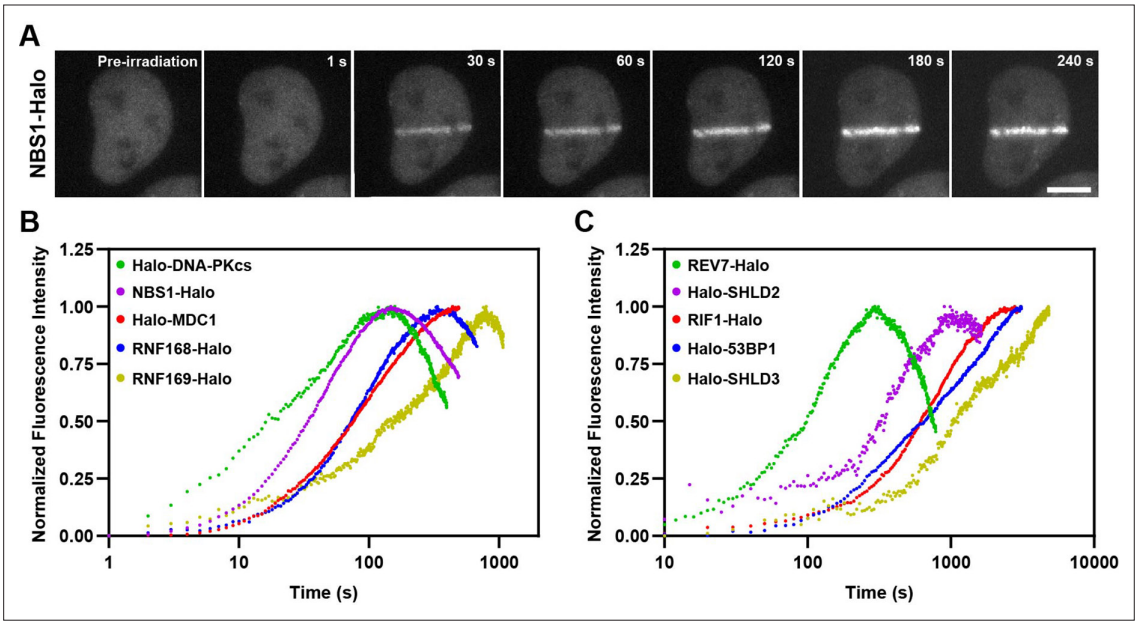

Figure 4. Kinetics of HaloTagged DDR proteins recruitment to sites of laser microirradiation induced DNA breaks. (**A**) Representative images of NBS1-Halo (JFX650) recruitment to laser-induced DSBs over time (Scale bar = 10 μm). (**B**) Normalized recruitment kinetics of HaloTagged DNA-PKcs, NBS1, MDC1, RNF168, and RNF169 proteins to laser-induced DSBs. (**C**) Normalized recruitment kinetics of HaloTagged 53BP1, RIF1, REV7, SHLD2, and SHLD3 proteins to laser-induced DSBs. Data are presented as the average increase in fluorescence post-laser microirradiation normalized to the brightest average frame for each movie. n=8–13 individual cells analyzed for each HaloTag cell line.

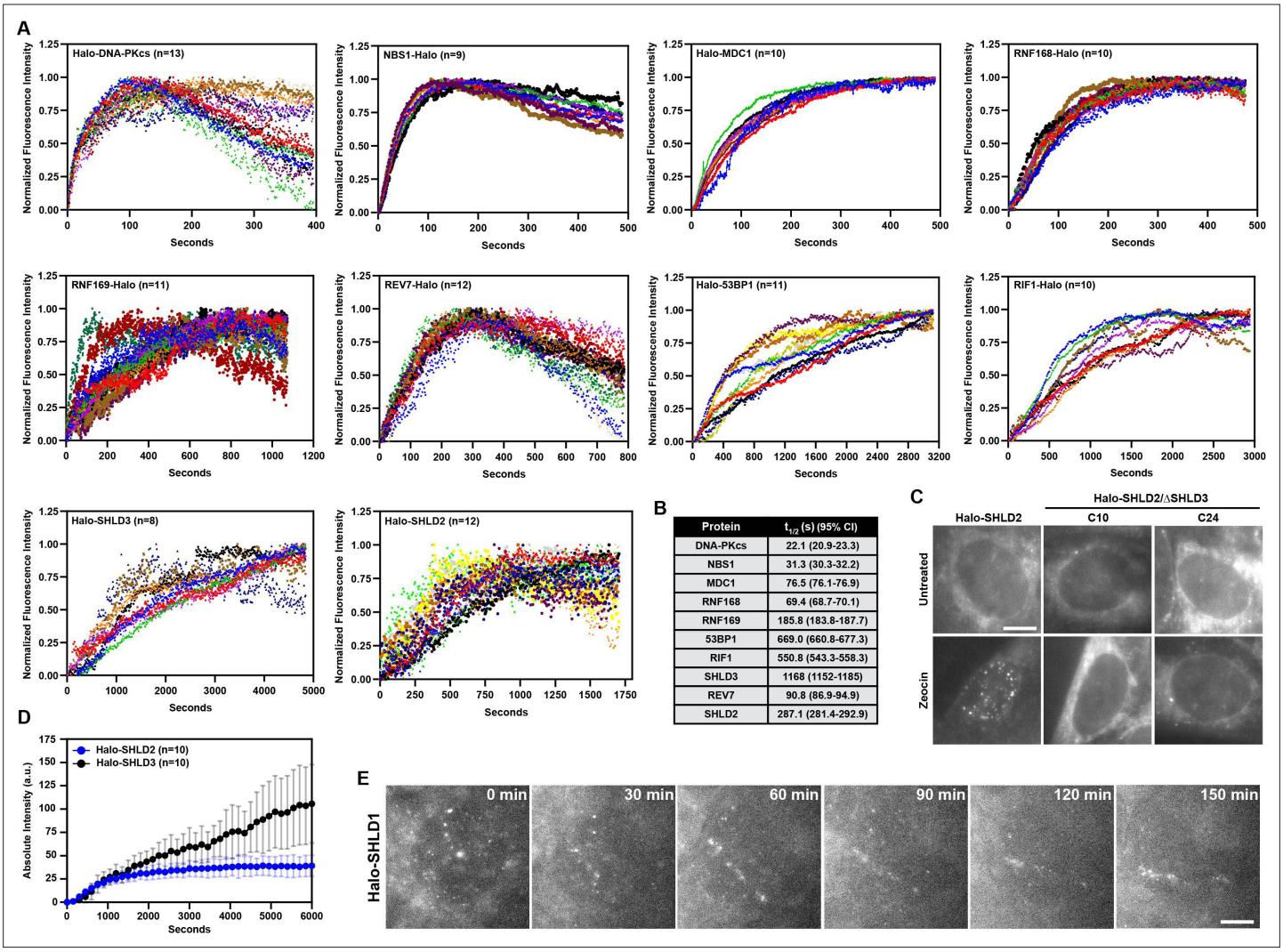

Protein	$t_{1/2}$ (s) (95% CI)
DNA-PKcs	22.1 (20.9-23.3)
NBS1	31.3 (30.3-32.2)
MDC1	76.5 (76.1-76.9)
RNF168	69.4 (68.7-70.1)
RNF169	185.8 (183.8-187.7)
53BP1	669.0 (660.8-677.3)
RIF1	550.8 (543.3-558.3)
SHLD3	1168 (1152-1185)
REV7	90.8 (86.9-94.9)
SHLD2	287.1 (281.4-292.9)

Figure 4—figure supplement 1. Kinetics of HaloTagged DDR protein recruitment to laser-induced DSBs. (**A**) Plots showing normalized fluorescence intensity and recruitment of each HaloTagged DDR protein to laser-induced DSBs plotted by individual cells rather than normalized average. Each color represents an individual cell that was analyzed. Normalized fluorescence intensity was done by setting the brightest frame for each cell to 1. (**B**) Table listing the recruitment half-times ($t_{1/2}$) of each protein to laser-induced DSBs determined by nonlinear regression assuming one-phase association. (**C**) Live-cell imaging of SHLD2 foci in SHLD3 +/+and SHLD3 -/- cells in the presence or absence of 100 µg/mL Zeocin. Scale bar = 5 µm. (**D**) Plot depicting the absolute fluorescence intensities of Halo-SHLD2 and Halo-SHLD3 recruitment to sites of laser-induced DNA damage. Data plotted as the average ± standard deviation. (**E**) Live-cell imaging of Halo-SHLD1 recruitment to DNA damage sites after laser microirradiation. Scale bar = 5 µm.

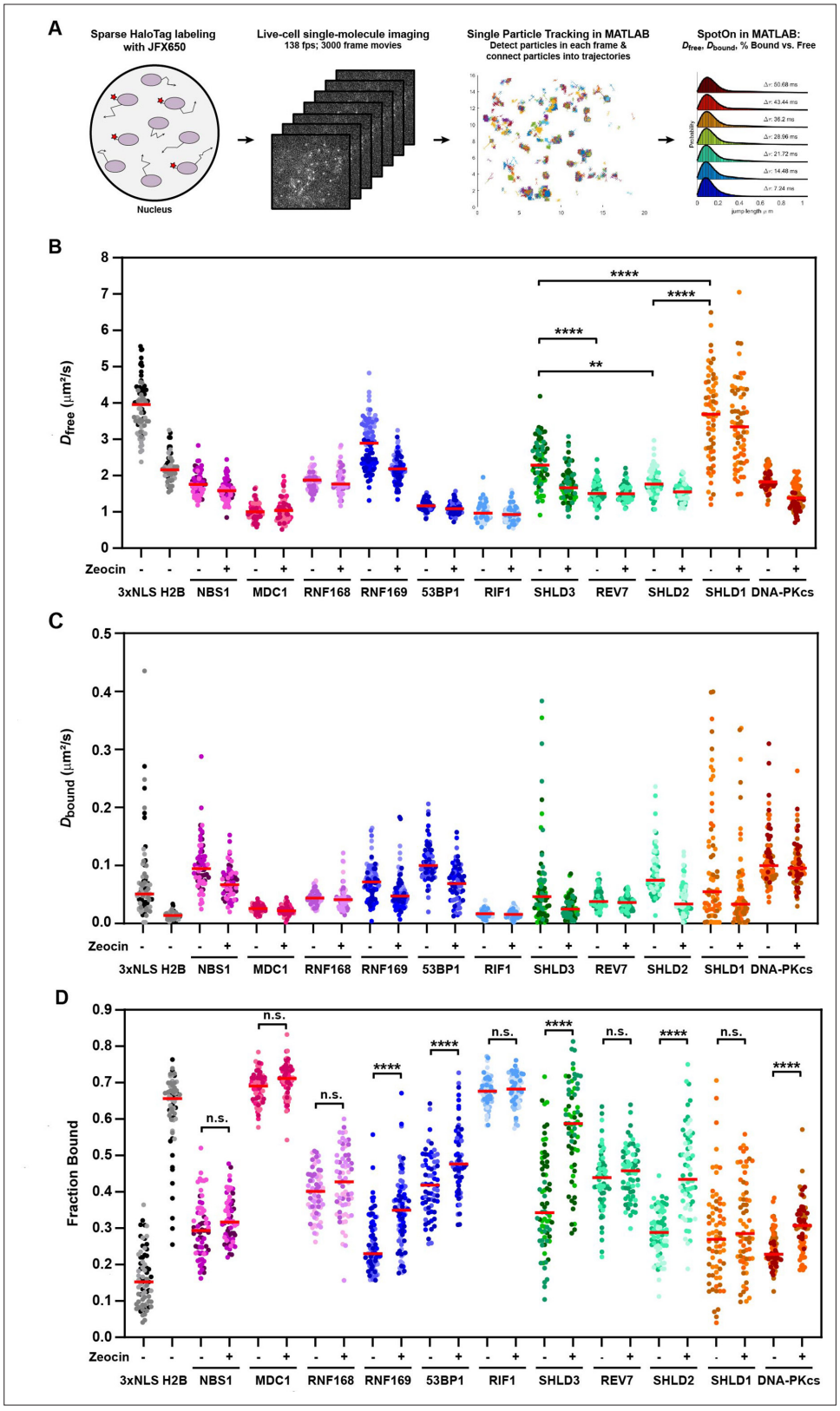

Figure 5. HaloTagged DDR proteins exhibit distinct nuclear diffusion and chromatin binding characteristics. (**A**) Graphical representation of the workflow used for live-cell single-molecule imaging of HaloTagged DDR proteins. (**B**) Diffusion coefficients for freely diffusing HaloTag DDR proteins present in at least three consecutive frames in untreated conditions and post-Zeocin exposure. Values plotted indicate the D_{free} for all analyzed tracks per cell

Figure 5 continued on next page

Figure 5 continued

with each dot indicating a separate cell that was analyzed. Live-cell single-molecule imaging was performed over 3–4 separate days imaging at least 20 individual cells per condition per experimental replicate (n≥60 cells total for each protein and condition representing three to four independent experiments). Red bar = median. (**C**) Diffusion coefficients of the bound fraction of HaloTag DDR proteins present in at least three consecutive frames in untreated conditions and post-Zeocin exposure. Values plotted indicate the D_{bound} for all analyzed tracks per cell with each dot indicating a separate cell that was analyzed. Live-cell single-molecule imaging was performed over 3–4 separate days imaging at least 20 individual cells per condition per experimental replicate (n≥60 cells total for each protein and condition). Red bar = median. (**D**) Plot of the Fraction Bound for each HaloTag DDR protein under each condition that were analyzed using a two-state model of diffusion. Each dot represents the fraction bound of each protein in an individual cell (n≥60 cells for each protein and condition). Red bar = median. Differently shaded points indicate data collected from separate biological experiments. Data were analyzed by two-way ANOVA with Tukey's posthoc test. n.s.=not significant. ** p=0.004; **** p<0.0001.

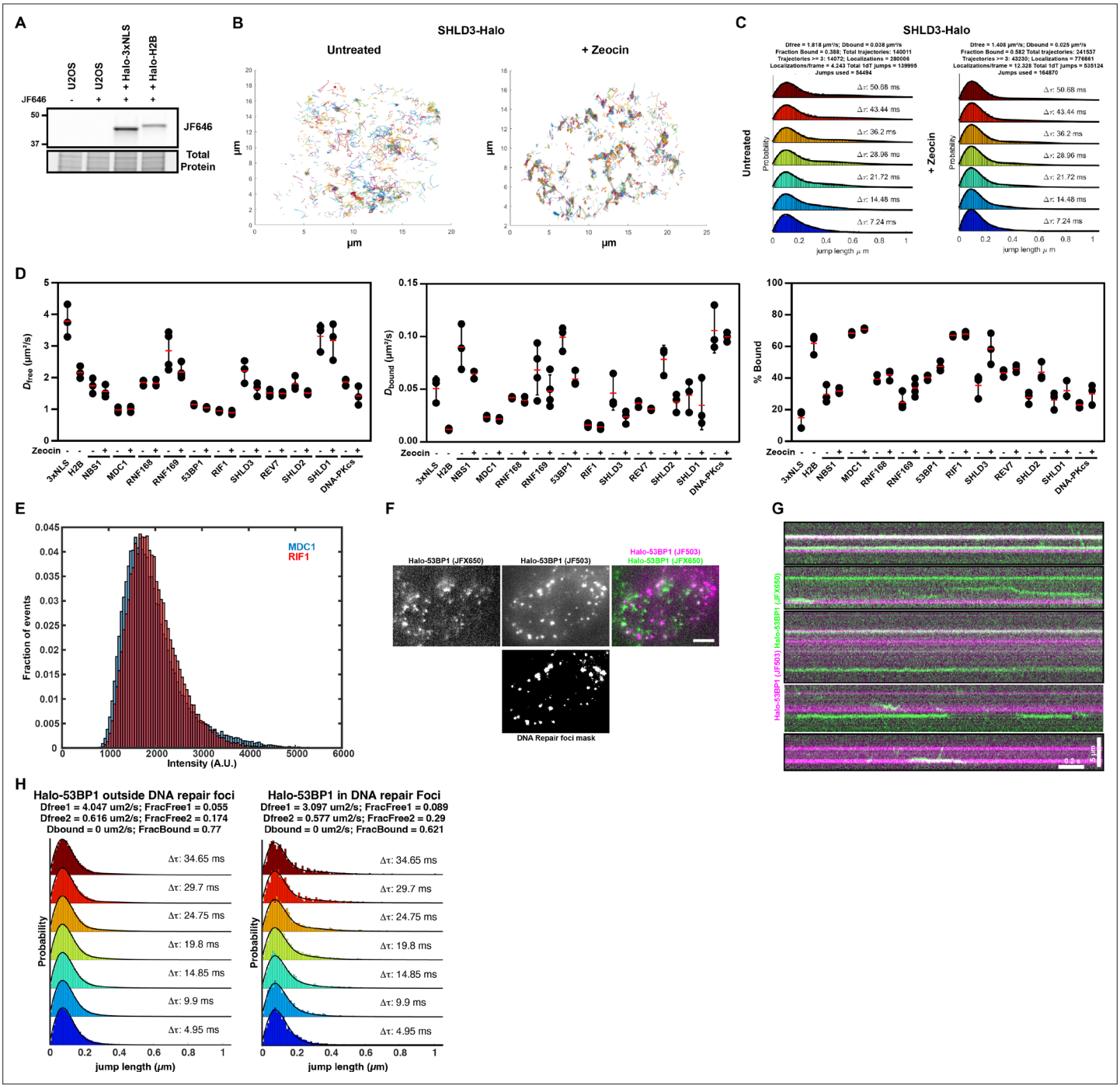

Figure 5—figure supplement 1. Nuclear diffusion and chromatin binding characteristics of HaloTagged DDR proteins. (**A**) SDS-PAGE gel showing expression of Halo-H2B and Halo-3xNLS in cells labeled with JF646. (**B**) Example images of protein tracks generated by single particle tracking of Halo-SHLD3 ±Zeocin. (**C**) Example plots from SpotOn for a single live-cell single-molecule experiment (>20 cells) for Halo-SHLD3 ±Zeocin. (**D**) Same data presented in ***Figure 5B & C***, except plotted by individual experiment, rather than as individual cells, to demonstrate the reproducibility of imaging between experiments. Each dot represents results from an individual experiment. Red bar = mean. Error bars = S.D. (**E**) Intensity profiles of analyzed tracks for JFX650-labeled MDC1 and RIF1. (**F**) Still frames Zeocin-treated Halo-53BP1 cells sparsely labeled with JFX650 (pseudo-colored green) and a Z-projected image of densely labeled Halo-53BP1 with JF503 (pseudo-colored magenta). Movies were acquired at 202 frames per second. Scale bar = 5 μm. (**G**) Kymographs of Halo-53BP1 (single-particles pseudo-colored green; foci pseudo-colored magenta) taken from ***Videos 23–24*** demonstrating distinct behaviors of 53BP1 particles inside and outside of foci. (**H**) SpotOn analysis using a three-state model of 53BP1 foci inside and outside of DNA repair foci. Tracks were filtered using the 53BP1 mask in (**F**).

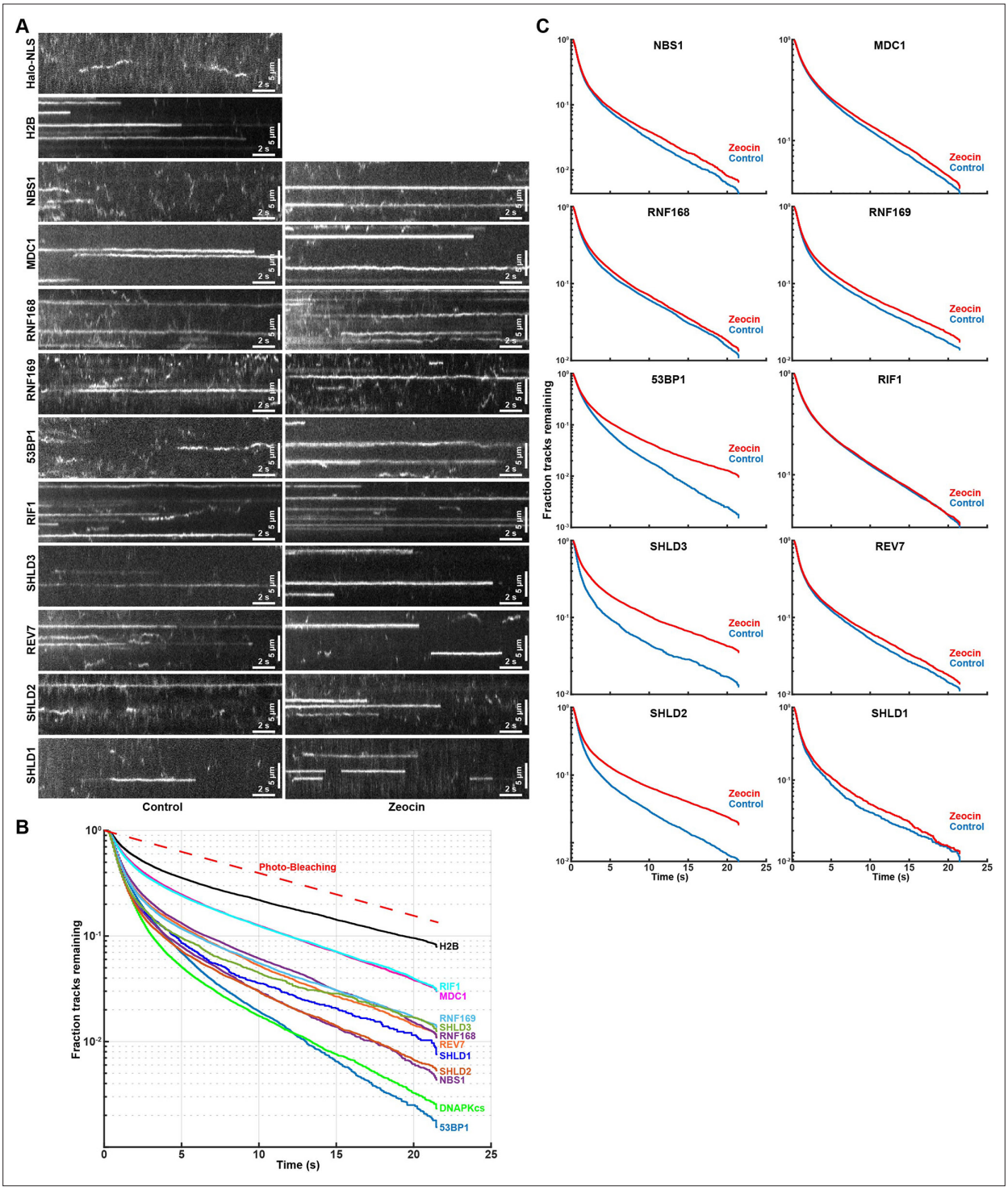

Figure 6. Residence time analysis of DNA repair factors in response to DNA damage. (**A**) Kymographs of single-molecule imaging movies for HaloTagged DNA repair factors. Movies were acquired with 7.2ms exposure times and to amplify long lasting interactions the intensity of 10 consecutive frames was averaged. (**B**) Residence time (track length) distribution of long-lasting chromatin binding events of DNA repair factors displayed as survival probability after the elapsed time. (**C**) Residence time (track length) distribution of long-lasting chromatin binding for the indicated DNA repair factors displayed as survival probability after the elapsed time. Aggregated data from 3 to 4 separate days imaging at least 20 individual cells per condition per experimental replicate (n≥60 cells total for each protein and condition) was fit with two exponential decay functions (R^2 >0.99 for all proteins) and half-lives and fractions of slow and fast decaying components are reported.

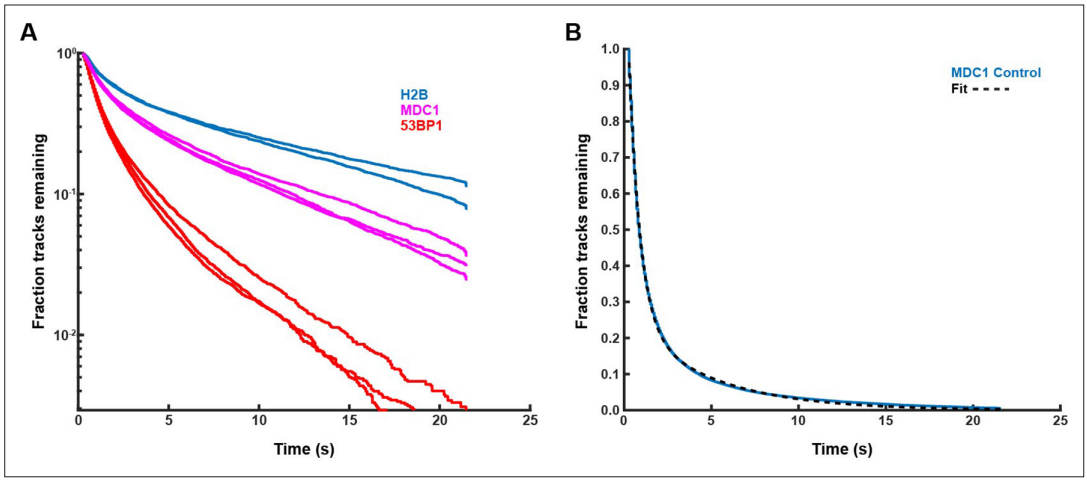

Figure 6—figure supplement 1. Residence time analysis of DNA repair factors in response to DNA damage. (**A**) Residence time (track length) distribution of long-lasting chromatin binding for the indicated DNA repair factors displayed as survival probability after the elapsed time. Graphs represent individual experimental replicates carried out on different days. (**B**) Residence time analysis for Halo-MDC1 fit with two exponential decay functions.

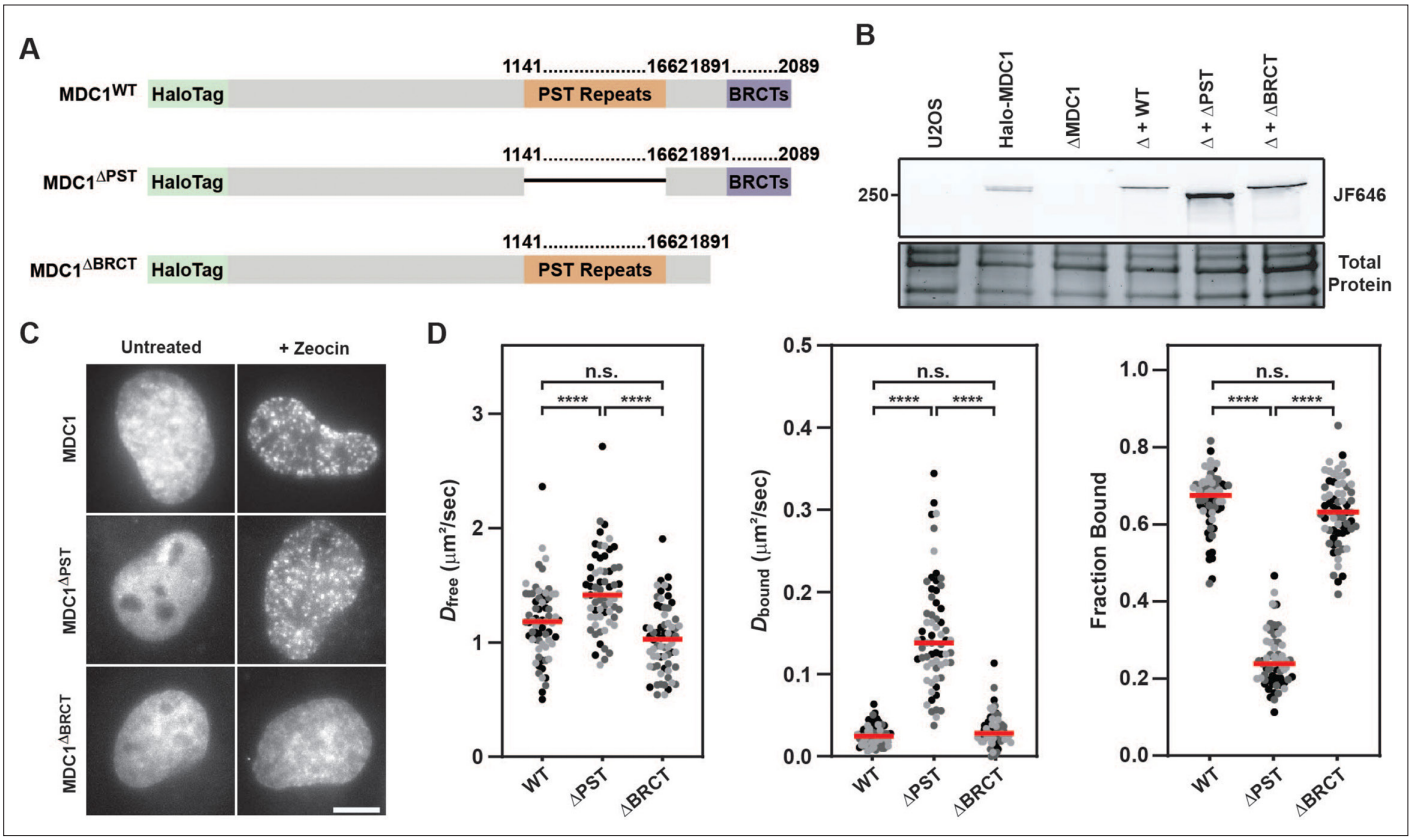

Figure 7. MDC1's constitutive chromatin association is mediated by its PST repeat region. (**A**) Graphical illustration of the primary sequence of MDC1 indicating the location of the PST repeat and BRCT domain and the associated deletion mutants generated to analyze effects on the MDC1-chromatin interaction. (**B**) SDS-PAGE gel of JF646-labeled cells depicting expression of transiently expressed WT, ΔPST, and ΔBRCT MDC1 in Halo-MDC1 knockout cells. (**C**) Representative images of transiently expressed, JF646-labeled MDC1 deletion mutants in living cells in the presence of absence of Zeocin. (**D**) Results of live-cell single-molecule analysis of transiently overexpressed MDC1 deletion mutants analyzed with single particle tracking and SpotOn. Each dot represents the indicated D_{free}, D_{bound}, or Fraction Bound for MDC1 molecules appearing in at least three consecutive frames within a single cell. Red bar = median. Data are the combination of all analyzed cells imaged over three independent experiments (n≥60 cells total). Differently shaded points indicate data collected from separate biological replicates. Data were analyzed by two-way ANOVA with Tukey's posthoc test. n.s.=not significant. ****=$p < 0.0001$.

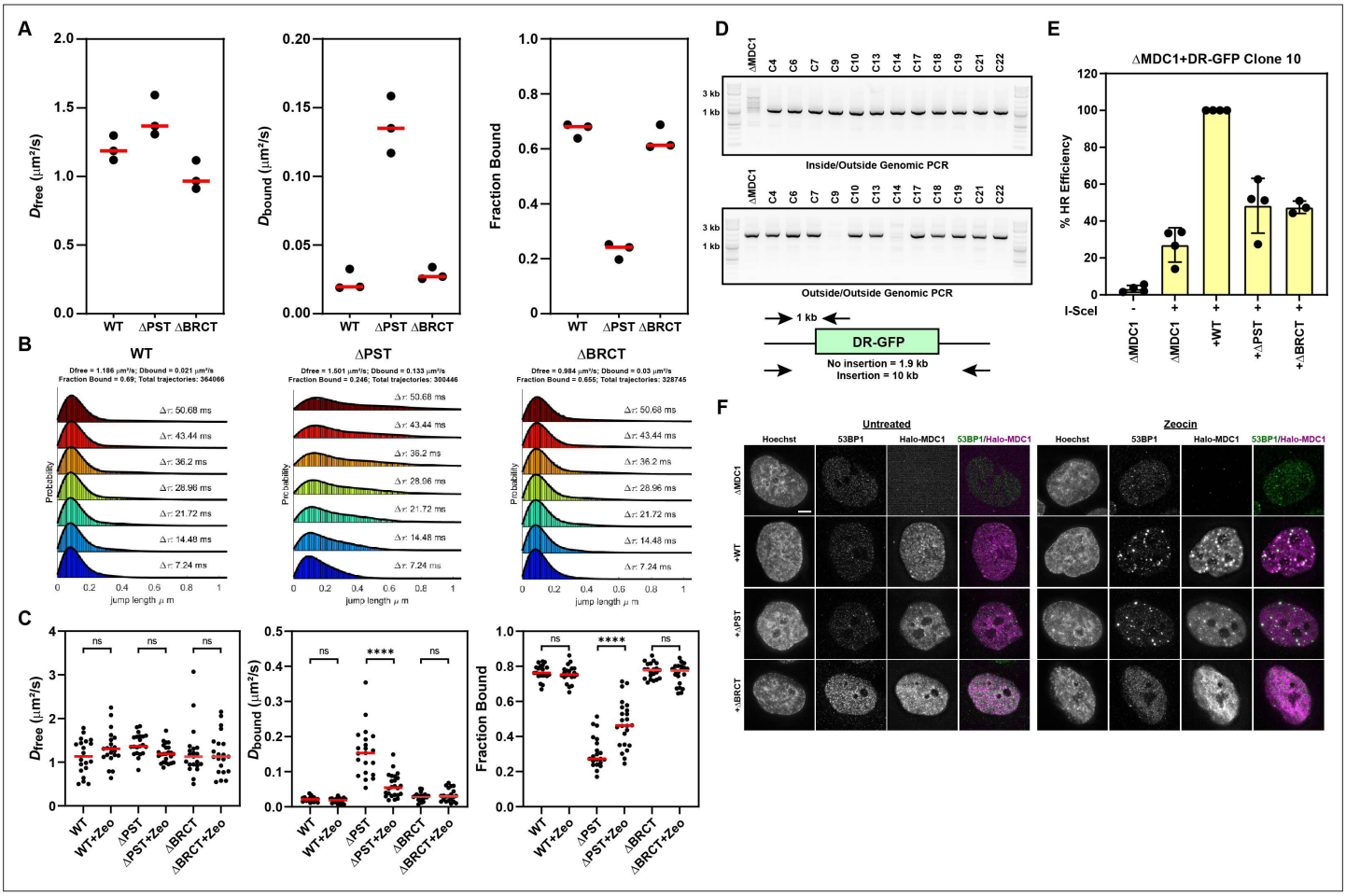

Figure 7—figure supplement 1. MDC1's constitutive chromatin association is mediated by its PST repeat region. (**A**) Same data presented in ***Figure 6D***, except plotted by individual experiment, rather than individual cells, demonstrating the reproducibility of analysis experiments. Each dot represents results from an individual experiment. Red bar = median. (**B**) Example plots generated by SpotOn for a single live-cell single-molecule experiment (>20 cells) of WT, ΔPST, and ΔBRCT MDC1. (**C**) Live-cell single-molecule imaging of MDC1 deletion mutants in untreated or after treatment with 100 µg/mL Zeocin (n≥20 cells per condition). Data compared by two-way ANOVA with Tukey's posthoc test. **** p<0.0001. (**D**) Genomic PCR demonstrating heterozygous knockin of the DR-GFP substrate into the *AAVS1* locus of ΔMDC1 cells. (**E**) Results from DR-GFP assay in ΔMDC1 cells transiently transfected with Halo-MDC1 mutants and I-SceI expression plasmid. (**F**) Immunofluorescence in ΔMDC1 cells transfected with HaloTagged MDC1 mutants ±10 µg/mL Zeocin treatment for one hour. Scale bar = 5 µm.